

# Convection in multiphase flows using Lattice Boltzmann methods

L. Biferale,<sup>1</sup> P. Perlekar,<sup>2</sup> M. Sbragaglia,<sup>1</sup> and F. Toschi<sup>3</sup>

<sup>1</sup>*Dept. of Physics and INFN, U. of Tor Vergata Via della Ricerca Scientifica 1, 00133 Rome, Italy*

<sup>2</sup>*Department of Physics and Department of Mathematics and Computer Science, Eindhoven University of Technology, 5600 MB Eindhoven, the Netherlands*

<sup>3</sup>*Department of Physics and Department of Mathematics and Computer Science, Eindhoven University of Technology, 5600 MB Eindhoven, the Netherlands and IAC, CNR, Via dei Taurini 19, 00185, Roma, Italy and INFN, via Saragat 1, I-44100 Ferrara, Italy.*

We present high resolution numerical simulations of convection in multiphase flows (boiling) using a novel algorithm based on a Lattice Boltzmann method. We first validate the thermodynamical and kinematical properties of the algorithm. Then, we perform a series of 3d numerical simulations at changing the mean properties in the phase diagram and compare convection with and without phase coexistence at  $Ra \sim 10^7$ . We show that in presence of nucleating bubbles non-Oberbeck Boussinesq effects develops, mean temperature profile becomes asymmetric, heat-transfer and heat-transfer fluctuations are enhanced. We also show that small-scale properties of velocity and temperature fields are strongly affected by the presence of buoyant bubble leading to high non-Gaussian profiles in the bulk.

PACS numbers: 47.20.Bp,47.55.-t

Thermal convection, the state of a fluid heated from below and cooled from above, is an ubiquitous phenomena in nature, present in many industrial and geophysical applications both at micro and macro-scales [1]. It is also challenging from the theoretical point of view, due to its extremely reach and different regimes ranging from intricate pattern formations at small temperature difference between bottom and top plates (i.e. moderate Rayleigh number) to extremely turbulent behavior where heat transfer and its adimensional definition (i.e. Nusselt number) is dominated by bulk or boundary layer physics (or by both, see e.g. recent reviews [2]). Most of the time thermal convection is studied in its simplest version, the so-called Oberbeck-Boussinesq (OB) approximation, where a single phase –unstratified– fluid is present with constant material properties. Compressibility is also neglected except for buoyancy forces. Needless to say, in many situation some, or all, of the above assumption breaks down and one enters in the realm of Non-Oberbeck-Boussinesq (NOB) convection. Deviations from OB can arises in many different way. Two notable cases are (i) the presence of stratification, as in many geophysical applications (ii) and under boiling conditions, i.e. when the parameters excursion inside the convective cell allows for phase coexistence [4, 5].

In this paper we address the latter case. We study thermal convection in a 3d cell in a high turbulent regime where large bubbles (larger than the turbulent viscous scale) can nucleate in the layer close to the bottom wall with a non-negligible heat-exchange between liquid and vapor. To do that, we present, validate and apply a novel numerical scheme based on a diffuse interface Lattice Boltzmann method (LBM) [3, 7]. We are not restricted to treat bubbles as point-like [8] and we fully resolve the thermo hydrodynamical properties of the gas

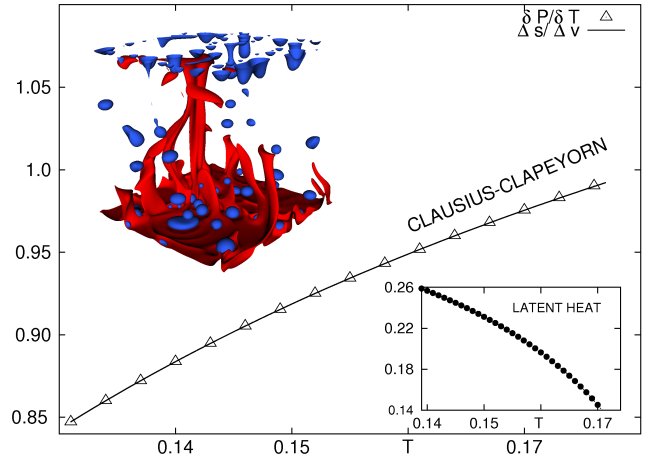


FIG. 1: Check of Clausius-Clapeyron relation  $\frac{\partial P}{\partial T} = \frac{\Delta s}{\Delta v}$  in our numerical scheme at varying  $T/T_c$ .  $P$  is the equilibrium pressure at coexistence temperature  $T$ ,  $v = 1/\rho$  is the specific volume,  $T_c$  is the critical temperature and  $s(T, \rho)$  is the specific entropy. Bottom inset: latent heat,  $\lambda = T\Delta s$  vs  $T$ . Top inset: Bubbles are in blue. Regions with high temperature are in red. The system has no-slip velocity at bottom and top walls and it is periodic on the horizontal directions.

and liquid phases. Beside the methodological aspects, we also address physical questions connected to the enhancement/depletion of heat flux in presence of bubbles, statistics of mean global properties as well as small-scales effects for both velocity and temperature fluctuations. We present two series of high-resolution numerical simulations up to  $512^3$  collocation points at  $Ra \sim 10^7$  with and without phase coexistence, such as to be able to directly compare on the same geometrical set up the effect

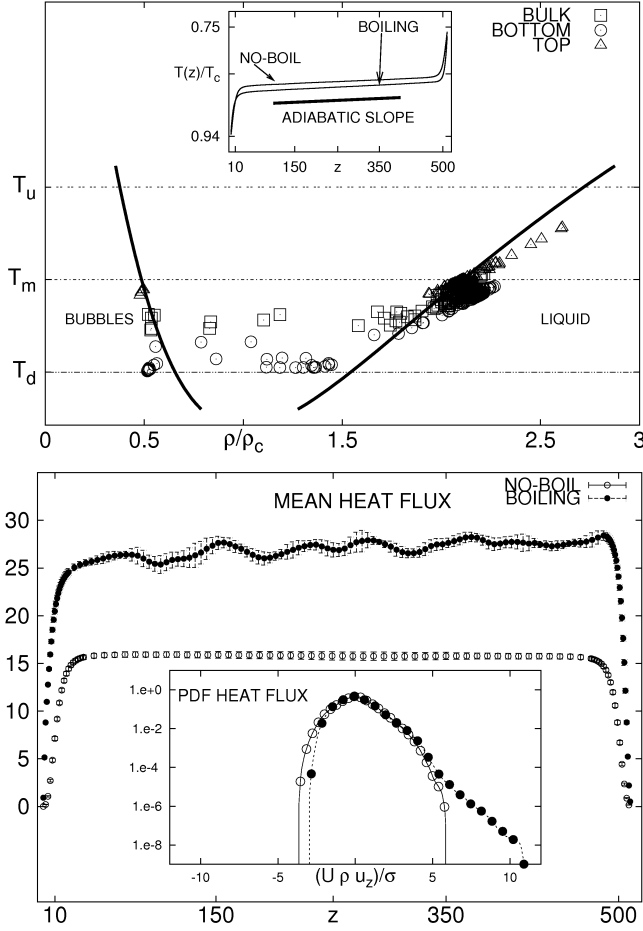


FIG. 2: TOP PANEL. Phase space  $T - \rho$  equilibrium curves (solid lines) superposed with a scatter plot of temperature and density values measured under boiling condition (both made dimensionless using the critical values,  $T_c$  and  $\rho_c$ ). Notice the presence of bubbles with different temperature inside the volume. Different symbols corresponds to measurements taken in top, bottom or bulk region. The horizontal dashed line correspond to top,  $T_u$ , bottom,  $T_d$ , and mean,  $T_m$ , temperatures. Inset: mean temperature profile,  $\overline{T(z)}/T_c$  vs  $z$  (in lattice units) for boiling and non-boiling conditions. The straight line corresponds to the adiabatic slope. BOTTOM PANEL. Bulk contribution to the heat flux normalized to its diffusive value,  $\overline{\rho U u_z}/[\kappa(T_d - T_u)/L]$ , (Nusselt) for boiling and non-boiling case at comparable Rayleigh number. Inset: pdf of  $\rho U u_z$  normalized to have mean area and mean variance for both boiling and non-boiling cases.

of boiling on convection. With respect to experimental studies, numerical simulations offer the unique advantages to allow access to all quantities without affecting the fluid dynamics and to confine the fluid inside “ideal” surfaces (i.e. perfect thermal properties at the wall, perfect smoothness of the boundaries etc...) On the other hand, a limitation consists in the difficulty to reach high Rayleigh numbers and to push the physical parameters as

density contrast, interface thickness, viscosity and thermal diffusivity to realistic situations. This is why the interplay between numerical investigations and experiments is crucial in this field.

The equations of motion describing a non-ideal fluid in presence of thermal fluctuations are:

$$\partial_t \rho u_i + \partial_j (\rho u_i u_j) = -\partial_i P + \partial_j (\mu (\partial_i u_j + \partial_j u_i)) + g \rho \hat{z} \quad (1)$$

where  $\mu = \rho \nu$  is the molecular viscosity,  $g$  is the gravity,  $\rho$  is the local fluid density and  $P(\rho, T) = P_0(\rho, T) + P_{NI}(\rho)$  is the non-ideal pressure. Pressure is fixed by the equation of state and it is made of two terms, the ideal part  $P_0(\rho, T) = \rho T$  and the non ideal part which in our LBM system reads:  $P_{NI}(\rho) = G \exp(-2/\rho)$  (see below). The equation for the internal energy,  $U = c_v T + \int d\rho P_{NI}/\rho^2$  is given by:

$$\rho D_t U + P \partial_j u_j = \kappa \partial_{jj} T \quad (2)$$

where  $\kappa$  is the thermal conductivity. The above equation can also be rewritten as one of the two following equivalent expressions:

$$\begin{cases} c_p \rho D_t T - \beta T D_t P = \kappa \partial_{jj} T \\ c_v \rho D_t T + P_0 \partial_j u_j = \kappa \partial_{jj} T \end{cases} \quad (3)$$

where  $D_t$  stands for the material derivative,  $c_v$  is the specific heat at constant volume,  $c_p$  and  $\beta = -(\partial_T \rho)/\rho$  are the specific heat and compressibility at constant pressure, respectively. The above set of equations tends to the usual OB system when the fluid is considered single phase, incompressible and both  $\mu, \kappa$  are constant [6]. In table 1 we report the characteristic values for all relevant parameters, with and without boiling.

Because of bubble nucleation/evaporation, a key role is played by the  $D_t P$  term in (3). Take for example a convective cell of eight  $L$  with imposed temperature,  $T_d$ , at the bottom wall and  $T_u$  at the top wall. Then, the heat balance across an horizontal layer at distance  $z$  from the bottom wall is given by the expression:

$$\partial_t \overline{\rho U}|_z + \partial_z \overline{\rho U v_z} - \kappa \partial_z \overline{T}|_z = -\overline{P \partial_j u_j}|_z \quad (4)$$

where with  $\overline{(\cdot)}|_z$  we intend a spatial average at fixed  $z$ . In a stationary situation, we can define a  $z$ -dependent dimensional Nusselt number  $Nu(z) = \overline{\rho U v_z} - \kappa \partial_z \overline{T}|_z$  which satisfy an integral constraint

$$Nu(z) - Nu(0) = - \int_0^z dz' \overline{P \partial_j u_j}|_{z'}. \quad (5)$$

With the above definition, the Nusselt number is not anymore constant throughout the cell, we may exchange heat by nucleating and evaporating bubbles or by simple compressible effects inside each phase.

ALGORITHM. The numerical algorithm used is based on discrete kinetic models [7]. The starting point is a

	$\Delta\tilde{T}$	$\Delta\tilde{c}_p$	$\chi_g$	$\chi_l$	$\nu$	$Ra$	$\Delta\tilde{\beta}$	$Pr$
BOILING	0.226	1.2	0.008	0.0018	0.0165	$3 \times 10^7$	1.6	9
NO-BOIL.	0.230	0.2	--	0.0018	0.0165	$2 \times 10^7$	0.1	9

TABLE I:  $\Delta\tilde{T}$ ,  $\Delta\tilde{c}_p$ ,  $\Delta\tilde{\beta}$ : values of temperature, liquid heat capacity and liquid compressibility difference between the two walls (all normalized with their respective values at the center of the cell,  $z_c$ ).  $\chi_{l,g} = \kappa/(c_p(z_c)\rho_{l,g}(z_c))$ : thermal diffusivity of liquid (l) and gas (g).  $\nu$ : kinematic viscosity. Rayleigh  $Ra$  and Prandtl  $Pr$  numbers are evaluated at  $z_c$  and in the liquid phase:  $Ra = \frac{g\beta(z_c)L^4(\Delta T/L - \gamma_{ad}(z_c))}{\kappa/(\rho(z_c)c_p(z_c))\nu}$  and  $Pr = \frac{\nu}{\chi^{(l)}(z_c)}$  where  $L = 512$  is the cell height (in grid units) and  $\gamma_{ad} = \beta T g/c_p$  is the adiabatic gradient. The Jacob number quantifying the ration between the sensible heat and the latent heat [8] is  $Ja \sim 3$ .

standard coupled mesoscopic dynamics described by [7, 9]:

$$f_l(\mathbf{x} + \mathbf{c}_l, t + 1) - f_l(\mathbf{x}, t) = -\frac{1}{\tau_\nu}(f_l - f_l^{(eq)})(\mathbf{x}, t) \quad (6)$$

$$g_l(\mathbf{x} + \mathbf{c}_l, t + 1) - g_l(\mathbf{x}, t) = -\frac{1}{\tau_\kappa}(g_l - g_l^{(eq)})(\mathbf{x}, t) \quad (7)$$

where  $f_l(\mathbf{u}, t)$ ,  $g_l(\mathbf{x}, t)$  stand for the probability density functions to find at  $(\mathbf{x}, t)$  a particle whose kinetic velocity belongs to a discrete and limited set  $\mathbf{c}_l$  (with  $l = 1, 19$  in the  $D3Q19$  LBM adopted here [7]). Density, momentum and temperature are defined as coarse-grained (in velocity space) fields of the distribution functions

$$\rho = \sum_l f_l \quad \rho \mathbf{u} = \sum_l \mathbf{c}_l f_l \quad \rho T = \sum_l g_l. \quad (8)$$

The local kinetic equilibria  $f_l^{(eq)}(\mathbf{u}', \rho)$  and  $g_l^{(eq)}(\mathbf{u}, \mathbf{F}, T)$  are usually expanded in suitable polynomial basis [10] in such a way that a Chapman-Enskog expansion [9] leads to the equations for density, momentum and temperature (1)-(3): the streaming step on the left hand side of (6) reproduces the inertial terms in the hydrodynamical equations, whereas dissipation and thermal diffusion are connected to the relaxation (towards equilibrium) properties in the right hand side, with  $\nu$  and  $\kappa$  related to the relaxation times  $\tau_\nu$ ,  $\tau_\kappa$  [7]. Non ideal thermodynamics is obtained by a well controlled procedure shifting the velocity in the equilibrium distribution,  $\mathbf{u}' = \mathbf{u} + \tau_\nu \mathbf{F}/\rho$ , with a forcing term mimicking the effect of an internal pseudo-potential [9, 10]. In particular, we adopt the standard form:

$$\mathbf{F} = -\mathcal{G} \sum_{l=1}^N w(|\mathbf{c}_l|^2) \mathbf{c}_l \psi[\rho(\mathbf{x})] \psi[\rho(\mathbf{x} + \mathbf{c}_l)] \quad (9)$$

where  $\mathcal{G}$  is a parameter dictating the overall strength of the non-ideal interactions. The weights  $w(|\mathbf{c}_l|^2)$  are used to enforce isotropy up to the 4th order in the velocity tensors [11]. The pseudo-potential,  $\psi[\rho]$ , encompasses the macroscopic effects of both long-range attraction and short-range repulsion. Although various choices

have been presented for the choice of  $\psi[\rho]$  [13, 14], here it is crucial to set it to  $\psi[\rho] = \exp(-1/\rho)$ , in such a way to reproduce the thermodynamic consistency on the lattice [12] (see fig. 1). Furthermore, to reproduce the correct ideal part of the pressure,  $P_0 = \rho T$ , a coupling between  $f_l$  and  $g_l$  populations in (3) is needed. To this end, we used a recent proposal [16] by plugging the dynamical temperature  $T$  extracted from the population  $g_l$  in the equilibrium distribution of (7): in the limit of vanishing interaction, this is equivalent to impose a second order momentum of  $f_l^{(eq)}$  equal to  $\sum_i f_l^{(eq)} c_i^i c_i^j = \rho T \delta_{ij} + \rho u_i u_j$ . Finally, in order to reproduce exactly the divergence term,  $P_0 \partial_j u_j$ , in (3), we found necessary to add a proper counter term to the evolution of  $g_l$  populations in (7), as proposed in [15]. As a result, we ended with a LBM scheme able to reproduce in the hydrodynamical limit the NS equations (1-3) with a non-ideal Pressure tensor and a consistent definition of latent heat (see fig. 1).

**SINGLE POINT QUANTITIES.** In fig. (2) we shown a scatter plot of  $T(\mathbf{x}, t)$  vs  $\rho(\mathbf{x}, t)$  for a boiling cell. As one can see most of the volume is at *thermodynamical equilibrium*, superposing with the equilibrium curves in the  $T - \rho$  phase space. The presence of bubbles is clearly detected by the spots concentrating along the vapor branch and it is also interesting to notice that the corresponding bubble temperature is always larger than the mean temperature in the cell, indicating that bubbles are transferring temperature upwards very efficiently. Moreover, the temperature profile across the cell,  $\bar{T}(z)$ , becomes slightly asymmetric in presence of bubbles, a phenomenon also observed in other liquid-like NOB systems [17]. Breaking of the top-down symmetry must not surprise. In particular,  $\beta$  is not constant across the cell (i.e. density and temperature fluctuations are not strictly proportional as in OB) and  $c_p$  decreases going from bottom to top. Both effects may have an impact on the averaged profiles as discussed and observed also in [17]. Here, the temperature mismatch between the values at the center and the mean temperature is 1% (inset of top panel in fig. 2). Notice also, in the same plot, that  $\bar{T}(z)$  agrees with the expected profile given by the adiabatic gradient, due to the presence of a small stratification.

In the bulk, the heat flux (5) is dominated by the convective term  $\rho \bar{U} u_z$ . In bottom panel of fig. (2) we compare the Nusselt number for the boiling and non-boiling cell at comparable Rayleigh. Two effects show up. First, heat flux is enhanced. Second, fluctuations around its mean profile are larger in presence of bubbles. We interpret this as a clear signature of the importance of the bubble dynamics in transporting heat between the two walls. This is the combined effect of temperature entrainment inside bubbles leveraged with the buoyancy effect that drift bubble upward much more efficiently than for plumes in single-phase convection. Because bubbles are

rare in our system, this also implies an increase in heat flux fluctuations, as can be seen in the inset of bottom panel in fig. (2) where we show the probability density function (pdf) of the heat flux measured only in the bulk cell. Clearly, the right tail are enhanced, due to bubble buoyancy. An open question is to see whether this enhancement of heat-flux is robust at changing Rayleigh and/or position in the phase diagram (with more or less bubble nucleation in the system). This needs to be investigated with new computational effort and will be reported in the future.

**SMALL-SCALES PROPERTIES.** Buoyant bubbles brings information from the physics of the bottom boundary layer in the bulk of the system. We then expect also in the bulk an increase of small scales fluctuations concerning both velocity and temperature fields. In fig. (3) we show the structure functions for vertical velocity and temperature:

$$\begin{cases} S_{u_z}^{(p)}(r) = \langle [u_z(\mathbf{x} + \mathbf{r}) - u_z(\mathbf{x}) \cdot \hat{\mathbf{r}}]^p \rangle_{bulk} \\ S_T^{(p)}(r) = \langle [T(\mathbf{x} + \mathbf{r}) - T(\mathbf{x}) \cdot \hat{\mathbf{r}}]^p \rangle_{bulk} \end{cases} \quad (10)$$

where the average is restricted on all points  $\mathbf{x}$  in the bulk of the cell and the increment  $\mathbf{r}$  is always taken in horizontal directions. In the two panels of fig.(3) we show the results for both quantities for  $p = 2$ . For both fields we have a viscous range very well resolved, where the structure functions goes as  $\propto r^2$ . Therefore, the presence of large-bubbles do not destroy the differentiability at small scales, another signature that the numerical set-up is under control. Second, boiling system have an enhanced signal at small scales, meaning that energy dissipation is globally increased. Third, for the boiling case we start to see an inertial range with K41-like scaling  $\propto r^{2/3}$ . In the inset of both panels we measure the Flatness (or Kurtosis) of each field  $K_{u_z, T}(r) = S_{u_z, T}^{(4)}(r) / [S_{u_z, T}^{(2)}(r)]^2$  at different scales, e.g. a way to quantify how much the pdf is close/different to a Gaussian. Intermittency, as measured by the deviation of the flatness from its Gaussian value,  $K = 3$  becomes more and more important at decreasing the scale, in agreement with the general observation that bubbles induce an increase of fluctuations in the system. For temperature (top panel fig. 3) the inertial range behavior is much more singular than the case for velocity, due to the enhancement of temperature jumps between inside and outside bubbles. At difference from the case for velocity, where large scale pdf is indistinguishable from a Gaussian ( $K_{u_z} \sim 3$  for  $r \sim L$ ), here temperature is more sensitive to the presence of bubbles also at large scale.

In conclusion, we have proposed and validated a novel LBM to attack multiphase flows with full consistent definition of heat exchange in the system (latent heat). We have applied this scheme to study convection under boiling condition and we have studied the effects of nucleating large bubbles at the bottom boundary layer on both

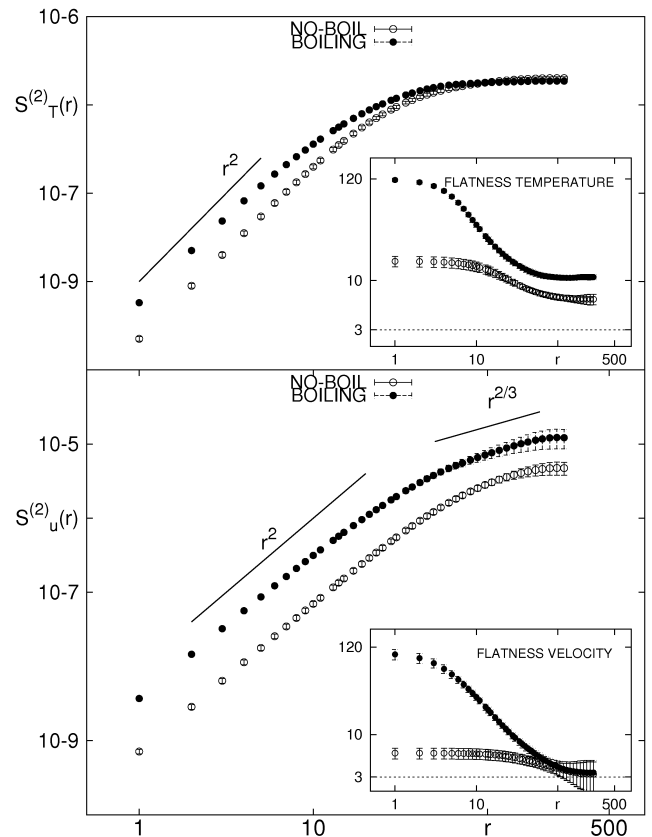


FIG. 3: 2nd order Structure Function for velocity (bottom) and temperature (top) vs  $r$  (in lattice units) for boiling and non-boiling systems. Inset: values of Flatness (same symbols))

single point observable (temperature profile and heat-flux) and two-point correlation functions (structure functions). The latter, allowed us to assess also the importance of bubbles on small-scales velocity and temperature fluctuations, indicating an enhancement of the deviations from Gaussian statistics with respect to the non-boiling case. We acknowledge useful discussion with R. Verzicco. The COST Action MP0806 is kindly acknowledged. Support within the DEISA Extreme Computing Initiative is acknowledged (FP6 project RI-031513 and FP7 RI-222919).

- 
- [1] P. Cardin & P. Olson, *Phys. of The Earth and Planetary Interiors* **82**, 235259 (1994); G.A. Glatzmaier & P. H. Roberts, *Nature* **377**, 203209 (1995).
  - [2] E. Bodenschatz, W.Pesch & G. Ahlers, *Annu. Rev. Fluid Mech.* **32**, 709-778 (2000); G. Ahlers, S. Grossmann & D. Lohse, *Rev. Mod. Phys.* **81**, 503 (2009).
  - [3] R. Zhang and H. Chen, Lattice Boltzmann method for simulations of liquid-vapor thermal flows, *Phys. Rev. E*

- 67, 066711, (2003).
- [4] J.-Q. Zhong, D. Funfschilling & G. Ahlers, *Phys. Rev. Lett.* **102**, 124501 (2009)
  - [5] V.K. Dhir, *Annu. Rev. Fluid Mech.* **30**, 365401 (1998)
  - [6] A. Spiegel & G. Veronis, *Astrophys. J.* **131**, 442 (1960).
  - [7] S. Succi, *The Lattice Boltzmann Equation* (Oxford Science, New York, 2001).
  - [8] P. Oresta et al., *Phys. Rev. E* **80**, 026304 (2009)
  - [9] B. Shi & Z. Guo, *Phys. Rev. E* **79** 016701 (2009); Z. Guo, C. Zheng & B. Shi, *Phys. Rev. E* **65**, 046308 (2002)
  - [10] X. Shan & H. Chen, *Phys. Rev. E* **47**, 1815 (1993); Sbragaglia et al., *Jour. Fluid. Mech.* **628**, 299 (2009)
  - [11] M. Sbragaglia et al. *Phys. Rev. E* **75**, 026702 (2007)
  - [12] M. Sbragaglia & X. Shan, *Phys. Rev. E* **84**, 036703 (2011)
  - [13] P. Yuan & L. Schaefer, *Phys. Fluids* **18**, 042101 (2006)
  - [14] A. L. Kupershtokh , D. A. Medvedev & D. I. Karpov, *Computers and Mathematics with Applications* **58**, 965974 (2009)
  - [15] N.I. Prasianakis & I.V. Karlin, *Phys. Rev. E* **76**, 016702 (2007)
  - [16] J. Zhang & F. Tian, *Europhys. Lett.* **81**, 66005 (2008)
  - [17] Ahlers et al., *Phys. Rev. E* **77**, 046302 (2008); *J. Fluid Mech.* **569**, 409445 (2006).